

Characterization of a Bifacial Silicon Solar Cell Under Multispectral Steady State Illumination Using Finite Element Method

Nzonzolo^{1, *}, Desire Lilonga-Boyenga¹, Camille N. Mabika¹, and Gregoire Sissoko²

Abstract—In this paper, we present results of characterization of a bifacial silicon solar cell, under multispectral steady state illumination, using finite element method (FEM). The illumination level (n) and back surface recombination velocities (Sb) effects on solar cell electrical parameters have been highlighted. After solving the continuity equation that describes the solar cell operation, the excess minority carrier's density and current-voltage characteristics are determined for various values of illumination level and recombination velocities on the junction and the back surface of the solar cell. The results obtained are in agreement with those given by analytical methods and prove that the photovoltaic cells can be analyzed only by numerical methods, such as the FEM, characterized by their robustness and flexibility in their applications in a context where those methods take more and more importance in the development of Computer Aided Design (CAD) tools.

1. INTRODUCTION

The studies carried out until now on the characterization of photovoltaic cells have been based, for majority of the cases, on the analytical methods [1–4] which, for certain transcendent equations for example, present many limits.

To solve this kind of equations, one often draws on graphic methods. Nowadays, numerical methods gain more and more importance. Several types of these methods have been implemented in simulation software. The equations which govern the operation of the photovoltaic cells are differential equations and can be solved numerically by taking account of the boundary conditions although they are particularly opposite to those usually used.

The objective of this study is to characterize a photovoltaic cell by the finite element method. Using this method, one-dimensional continuity equation will be solved, and the excess minority carrier's density versus the base depth will be determined for various values of the back surface recombination velocity Sb , junction recombination velocity Sj , and illumination level n . The photocurrent density and photo voltage will also be determined as well as the current-voltage characteristics of the photovoltaic cell. Finally, the results obtained by the finite element method will be compared with those obtained by the analytical approach.

2. THEORETICAL ANALYSIS

Let us consider a bifacial silicon solar cell, illuminated on its front surface then by its back surface as represented in Figure 1.

One designates the depth of the base by H and any position in the base by x .

Received 2 September 2016, Accepted 30 December 2016, Scheduled 23 January 2017

* Corresponding author: Nzonzolo (nzonzolo@gmail.com).

¹ Laboratoire d'Electronique et Electrotechnique Ecole Nationale Supérieure Polytechnique, Université Marien Ngouabi, Congo. ² Laboratoire des Semi-conducteurs et d'Énergie Solaire, Département de Physique, Faculté des Sciences et Techniques, Université Cheikh AntaDiop, Dakar Sénégal.

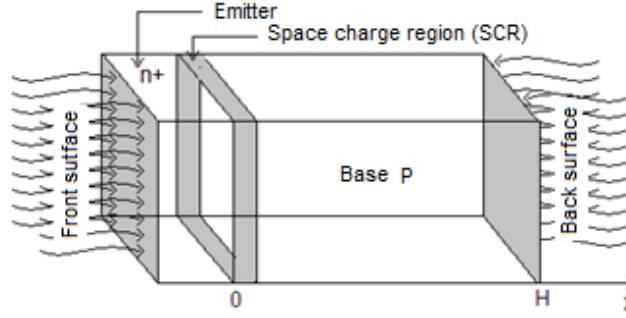


Figure 1. Silicon bifacial solar cell.

We consider the one-dimensional case assumption where all parameters depend only on x . The continuity equation which governs the solar cell operating is given by [5]:

$$\frac{\partial^2 \delta(x)}{\partial x^2} - \frac{\delta(x)}{L^2} = -\frac{g(x)}{D} \quad (1)$$

$\delta(x)$ is the excess minority carrier's density in the base, $L = \sqrt{D \cdot \tau}$ the diffusion length, D the diffusion constant, τ the lifetime of electrons, and $g(x)$ the generation rate of carriers.

This carrier's density is subjugated to the following boundary conditions:

- at the junction

$$D \cdot \frac{\partial \delta(x)}{\partial x} \Big|_{x=0} = S_j \cdot \delta(0) \quad (2)$$

- at the back surface,

$$D \frac{\partial \delta(x)}{\partial x} \Big|_{x=H} = -S_b \cdot \delta(0) \quad (3)$$

where S_j indicates the junction recombination velocity and S_b the back surface recombination velocity.

To solve Equation (1), we propose here to use the finite element method.

Let: $u(x) = \delta(x)$, $a = \frac{S_j}{D}$, $b = -\frac{S_b}{D}$, $c(x) = \frac{1}{L^2}$ and $f(x) = \frac{g(x)}{D}$, the continuity Equation (1) becomes:

$$-u''(x) + c(x) \cdot u(x) = f(x) \quad (4)$$

with its boundary conditions: $\begin{cases} u'(0) = a \cdot u(0) \\ u'(H) = b \cdot u(H) \end{cases}$.

These boundary conditions are mixed or Fourier and Neumann type [6], i.e. they imply the function u and its derivative u .

The carrier's generation rate of the solar cell illuminated by its front surface and back surface can be approached by the relation [5]:

$$g(x) = \begin{cases} \sum_1^3 n \cdot a_i \cdot \exp(-b_i x) \\ \sum_1^3 n \cdot a_i \cdot \exp(-b_i (H - x)) \end{cases} \quad (5)$$

The quantities a_i and b_i are the constants deduced from modeling of the generation rate considered for the overall solar radiation [5]. n stands for the illumination level.

u is a single solution of Equation (4), whose functional can be written:

$$F(u) = \int \left[\frac{1}{2} \left(\frac{\partial u}{\partial x} \right)^2 + \frac{cu^2}{2} - f(x) \cdot u(x) \right] dx - u(H)u'(H) + u(0)u'(0) \quad (6)$$

v being a test function, which leads to the variational form [6, 7] given by the following equation:

$$A(u, v) = L(v) \tag{7}$$

where A and L are defined by:

$$A(u, v) = \int_0^H u'(x) \cdot v'(x) dx + \int_0^H c(x) \cdot u(x) \cdot v(x) dx + a \cdot u(0) \cdot v(0) - b \cdot u(H) \cdot v(H) \tag{8}$$

and

$$L(v) = \int_0^H f(x) \cdot v(x) dx \tag{9}$$

To solve Equation (7), one subdivides the domain $[0, H]$ in N finite elements, where N is a positive integer, and $h = \frac{H}{N+1}$ is the step of discretization, i.e., the distance between two consecutive points, as shown in Figure 2.

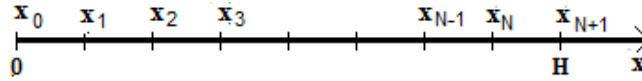


Figure 2. 1D discretization of the solar cell base depth.

Using the Galerkin method, one defines a space with finite dimensions which tends towards the interval $[0, H]$ when h tends towards zero.

According to the Lax-Milgram theorem, there exists a single solution u_h for the discrete variational problem.

u_h is the approximate solution which tends towards u when h tends towards zero.

If $\{\omega^i(x)\}$ is a base of trial functions suitably chosen, we can develop functions u and v on this basis. Thus:

$$u = \sum_{i=1}^{N+1} U_i \omega^i(x) \quad \text{and} \quad v = \sum_{j=1}^{N+1} V_j \omega^j(x)$$

The approximation of functions u and v respectively in the base of functions $\omega^i(x)$ and $\omega^j(x)$ permits the writing of Equation (7) in the form:

$$MU = L \tag{10}$$

where A and L are matrices of elements:

$$M_{i,j} = \int_0^H \left((\omega^i)'(x) \cdot (\omega^j)'(x) + c(x) \cdot \omega^i(x) \cdot \omega^j(x) \right) dx + a \cdot \omega^i(0) \cdot \omega^j(0) - b \cdot \omega^i(H) \cdot \omega^j(H) \tag{11}$$

$$U = (U_1, U_2, \dots, U_n) \tag{12}$$

and

$$L_i = \int_0^H f(x) \cdot \omega^i(x) dx \tag{13}$$

In many one-dimensional problems, function $\omega^i(x)$ has its support in $[x_{i-1}, x_{i+1}]$ and can be expressed as follows [7]:

$$\omega^i(x) = \begin{cases} \omega_1 \left(\frac{x - x_{i-1}}{h} \right) & \text{for } x \in [x_{i-1}, x_i] \\ \omega_0 \left(\frac{x_{i+1} - x}{h} \right) & \text{for } x \in [x_i, x_{i+1}] \\ 0 & \text{on the other intervals} \end{cases} \tag{14}$$

The basic functions ω_0 and ω_1 are given by: $\omega_0(x) = 1 - x$ and $\omega_1(x) = x$.

The solution of the continuity Equation (1) taking into account the boundary conditions is then given by:

$$U = M^{-1} \cdot L \quad (15)$$

This solution gives the density of photogenerated carriers from which the photocurrent density J and photo voltage V can be determined [5].

3. RESULTS AND DISCUSSION

The continuity equation is solved using a numeric code which we have conceived. In order to validate our calculations, we plot the profile of excess minority carrier's density versus base depth x . This profile is compared with that obtained by the analytical method before examining the effects of S_j , S_b and n .

3.1. Excess Minority Carriers' Density

3.1.1. Front Surface Illumination

When the solar cell is illuminated on its front surface, we obtain the profile of the carrier's density represented in Figure 3.

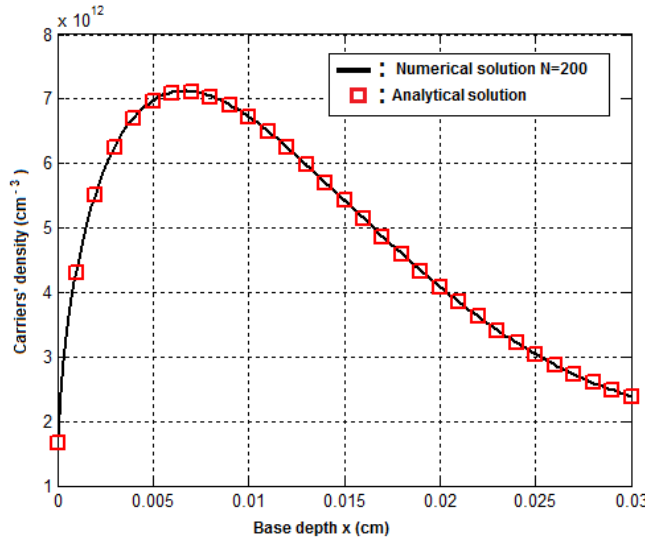


Figure 3. Minority carrier's density; $S_j = 10^5$ cm/s; $D = 26$ cm²/s; $L = 0.01$ cm; $S_b = 10^3$ cm/s, front surface illumination.

One notes a good agreement between these results and those given by analytical approach, when the number of finite elements is equal or superior to 200.

For this value of $N = 200$, we represent, in Figure 4, the minority carriers' density photogenerated for various values of the junction recombination velocity S_j .

We notice the reduction level and the displacement of the maximum of the carriers' density, due to the widening of the space charge region, when the junction recombination velocity increases.

This result is in conformity to that given by [1].

We are also interested in the profile of the minority carriers' density for various values of the back surface recombination velocity S_b , represented in Figure 5.

As envisaged, this density decreases when the back surface recombination velocity S_b increases.

To highlight the effectiveness of the finite element method, we represent, in Figure 6, the minority carriers' density for various values of illumination level n .

As shown in this figure, our results agree with those obtained analytically.

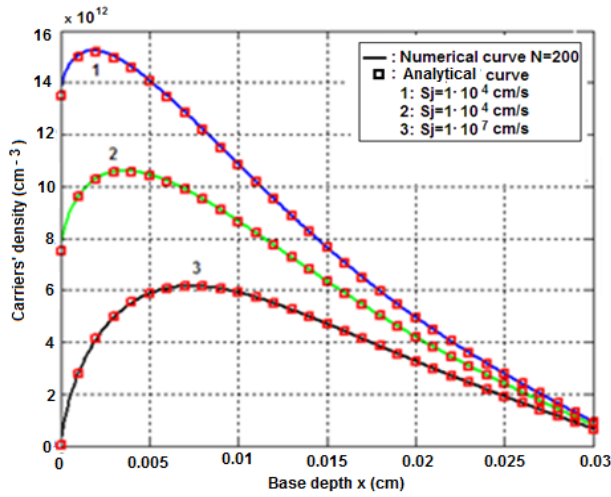


Figure 4. Minority carriers density for various junction recombination velocities S_j : $D = 26 \text{ cm}^2/\text{s}$; $L = 0.01 \text{ cm}$; $S_b = 10^3 \text{ cm/s}$, front surface illumination.

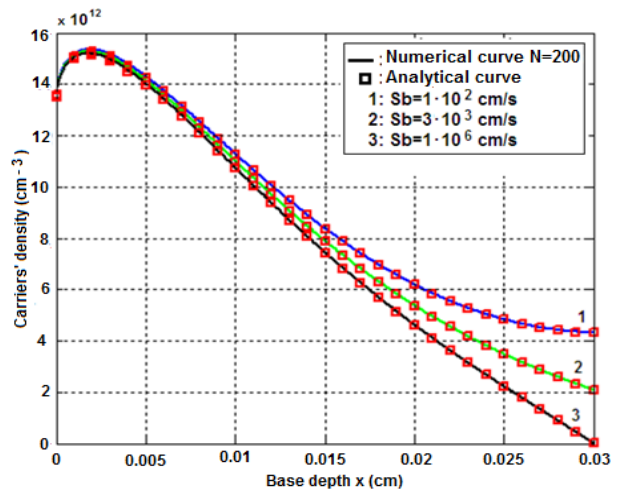


Figure 5. Minority carriers density for various junction recombination velocities S_b : $D = 26 \text{ cm}^2/\text{s}$; $L = 0.01 \text{ cm}$; $S_j = 10^3 \text{ cm/s}$, front surface illumination.

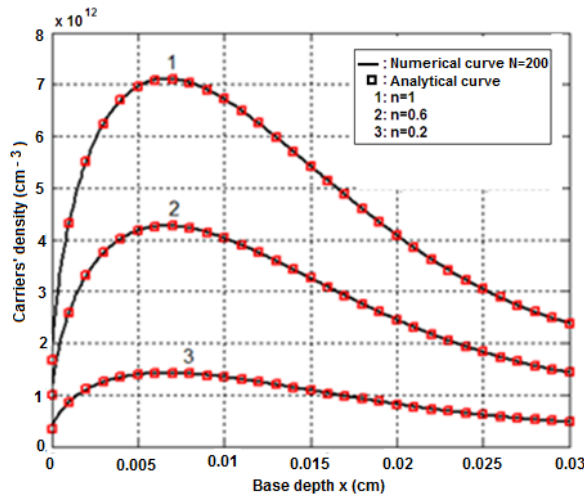


Figure 6. Minority carriers density for various back surface recombination velocities S_b : $D = 26 \text{ cm}^2/\text{s}$; $L = 0.01 \text{ cm}$; $S_j = 10^4 \text{ cm/s}$, front surface illumination.

3.1.2. Back Surface Illumination

For an illumination of the bifacial solar cell on the back surface, the profile of the minority carriers' density photogenerated is compared with that obtained by the analytical method. This profile is shown in Figure 7.

Contrary to the front surface illumination, the numerical solution is identical to analytical solution when the number of finite elements N is superior or equal to 500.

To obtain these results, it was necessary to consider much more finite elements ($N = 500$), when the solar cell is illuminated on its back surface, other than on its front surface. That can be explained by the fact that when the second member $g(x)$ of Equation (2) is not linear, the convergence of the solution requires greater number of finite elements.

With N fixed at 500, we also show the minority carrier's density photogenerated in Figure 8 and in Figure 9 respectively for various values of S_b and n .

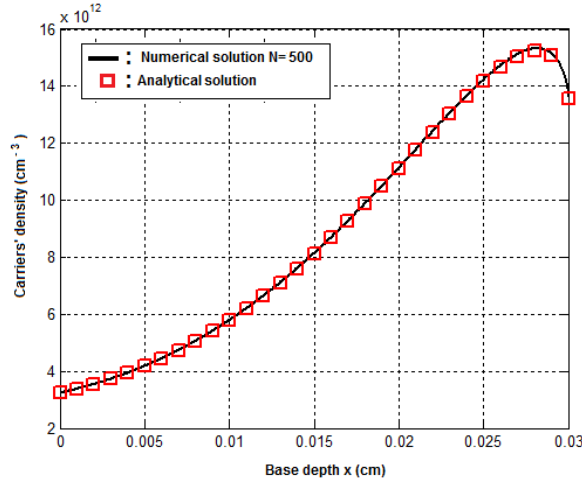


Figure 7. Minority carrier’s density; $D = 26 \text{ cm}^2/\text{s}$; $L = 0.01 \text{ cm}$; $Sb = 10^3 \text{ cm/s}$, back surface illumination.

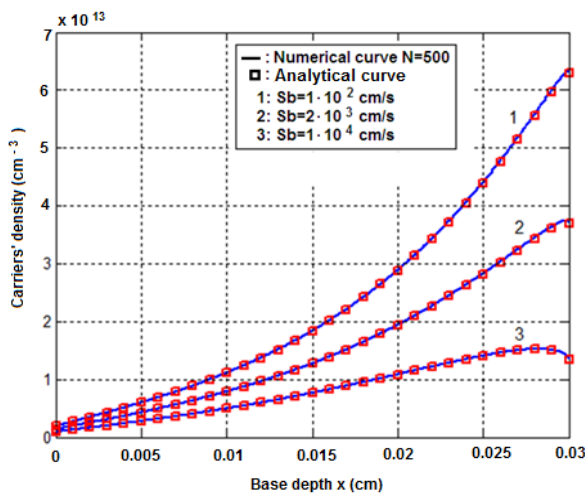


Figure 8. Minority carriers density for various back surface recombination velocities Sb : $D = 26 \text{ cm}^2/\text{s}$; $L = 0.01 \text{ cm}$; $Sj = 10^4 \text{ cm/s}$, back surface illumination.

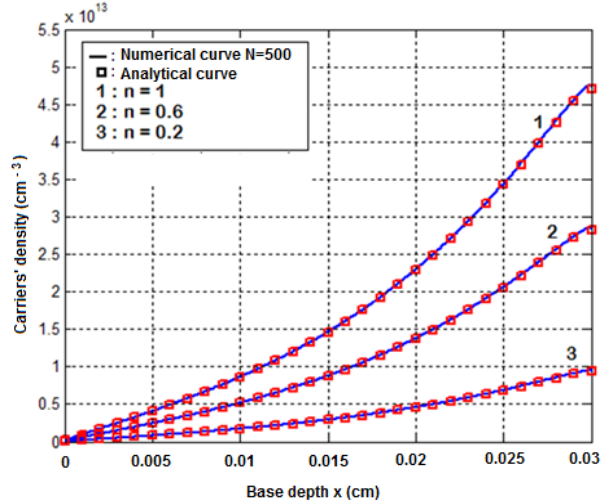


Figure 9. Minority carriers density for various values of n : $D = 26 \text{ cm}^2/\text{s}$; $L = 0.01 \text{ cm}$; $Sj = 10^5 \text{ cm/s}$, $Sb = 10^3 \text{ cm/s}$, back surface illumination.

It can be noted that the results of our simulations are identical to those obtained by the analytical method [1].

3.1.3. Simultaneous Illumination

The simultaneous illumination occurs when the bifacial solar cell is illuminated on its two surfaces. In the assumption that the junction recombination velocity and the back surface velocity are the same, as well as the value of illumination level n , we shown, in Figure 10, the minority carriers’ density photogenerated versus the base depth. This profile is compared with that obtained by the analytical method.

For this simultaneous illumination of the solar cell, the perfect agreement between the numerical solution and analytical solution is obtained when the number of finite elements N considered is superior or equal to 800. Here, $g(x)$ is the sum of both generation rates on front surface and back surface.

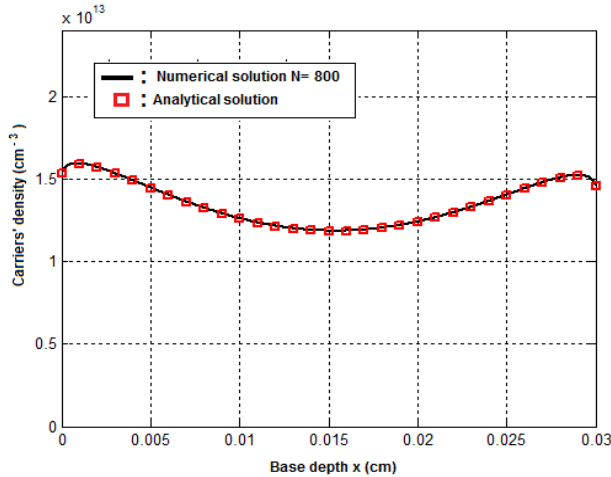


Figure 10. Minority carrier's density; $Sj = 10^4$ cm/s; $D = 26$ cm²/s; $L = 0.01$ cm; $Sb = 10^4$ cm/s, simultaneous illumination.

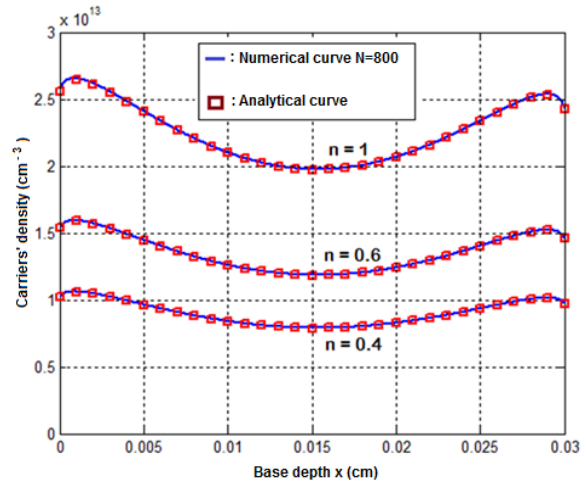


Figure 11. Minority carrier's density for various values of n : $D = 26$ cm²/s; $L = 0.01$ cm; $Sj = 4, 6 \times 10^3$ cm/s; $Sb = 5 \times 10^3$ cm/s, simultaneous illumination.

For this value of $N = 800$ and for various values of illumination level, the minority carriers' density is shown in Figure 11.

This minority carriers' density determined using the finite element method presents a profile which reflects exactly the solar cell working [1, 4].

These results are in conformity with those obtained by the analytical approach.

3.2. Photocurrent Density

In the aim of continuing the validation of our code, let us examine the behavior of photocurrent density when the solar cell is illuminated on the front surface. The numerically determined photocurrent density is compared with that obtained by the analytical method. These profiles are represented versus the junction recombination velocity Sj , in Figure 12.

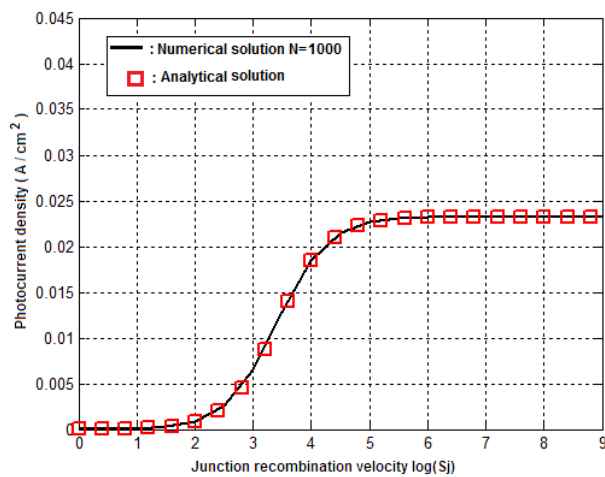


Figure 12. Photocurrent density versus Sj ; $D = 26$ cm²/s; $L = 0.01$ cm; $Sb = 10^3$ cm/s, front surface illumination.

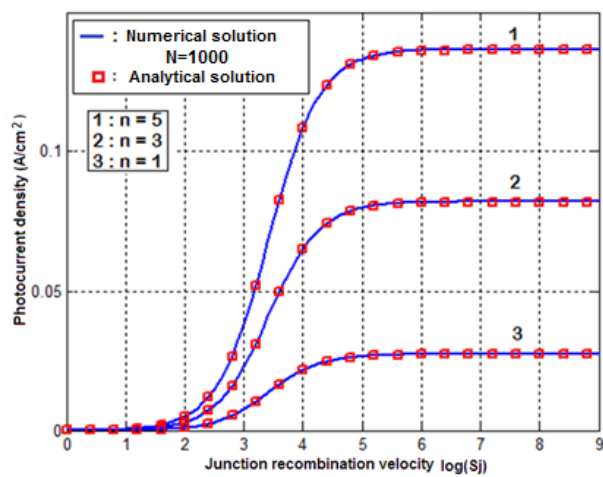


Figure 13. Photocurrent density versus Sj for various values of illumination level n : $D = 26$ cm²/s; $L = 0.01$ cm; $Sb = 10^3$ cm/s, front surface illumination.

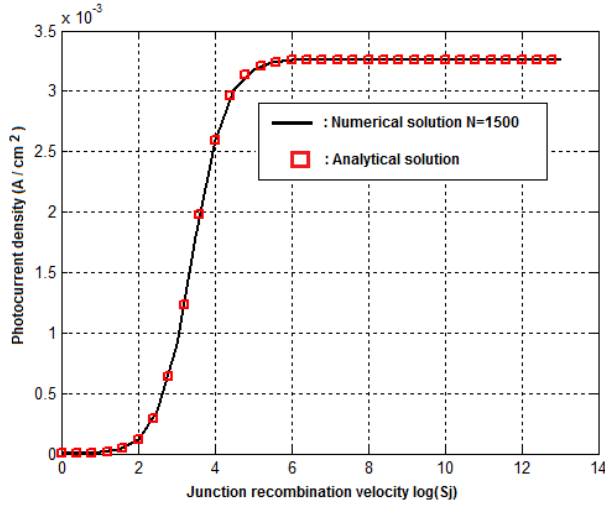


Figure 14. Photocurrent density versus Sj ; $D = 26 \text{ cm}^2/\text{s}$; $L = 0.01 \text{ cm}$; $Sb = 10^3 \text{ cm/s}$, back surface illumination.

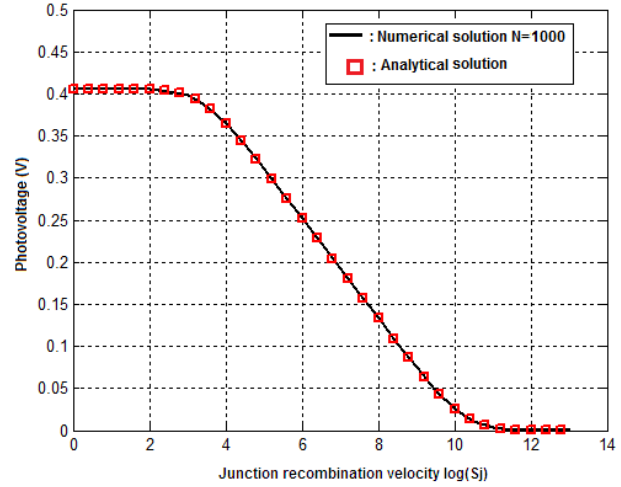


Figure 15. Photovoltage versus junction recombination velocity Sj ; $D = 26 \text{ cm}^2/\text{s}$; $L = 0.01 \text{ cm}$; $Sb = 10^3 \text{ cm/s}$, front illumination.

The perfect concordance between the numerical and analytical solutions is obtained when the considered number of finite elements N is superior or equal to 1000. For this value of N and various values of illumination level n , we show, in Figure 13, the photocurrent density. One notes that the current density increases with the illumination level n , and the obtained profiles are identical to those given by the analytical methods.

Figure 14 shows the photocurrent density versus junction recombination velocity, when the solar cell is illuminated on its back surface.

As shown in this figure, for the illumination of solar cell on its back surface, the numerical solution is close to the analytical solution when N is superior or equal to 1500.

3.3. Photovoltage

To validate our code of calculations, we are also interested in the photovoltage. Figure 15 shows the photovoltage versus junction recombination velocity (Sj). The photovoltage is compared with the profile of the analytical solution when the solar cell is illuminated on its front surface for $N = 500$.

One notes a perfect agreement between our results and analytical ones [8].

3.4. Current-Voltage Characteristics

For an illumination of a solar cell on its front surface, the current-voltage characteristic is shown in Figure 16, for $N = 1000$ finite elements of base depth discretization.

The agreement of our results with those obtained using analytical method is observed. As for the photocurrent density, we also show the current-voltage characteristic of the solar cell illuminated on its back surface, which is represented in Figure 17 for $N = 1500$. In fact, this illumination needs more finite elements.

The numerical results agree with the analytical ones when the number of finite elements is superior or equal to 1500 [9].

Thus we can note that for the low values of the voltage, the photocurrent is constant and corresponds to the short-circuit current. It decreases rapidly and cancels out when the open circuit voltage is reached. Moreover, the short-circuit photocurrent density is important for the front surface illumination [10].

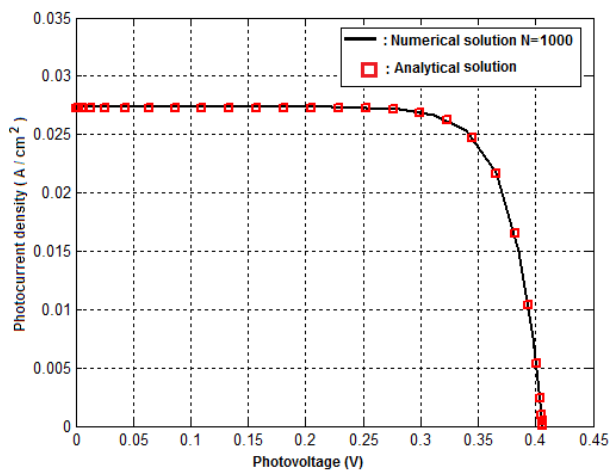


Figure 16. Current-voltage characteristics; $D = 26 \text{ cm}^2/\text{s}$; $L = 0.01 \text{ cm}$; $Sb = 10^3 \text{ cm/s}$, front surface illumination.

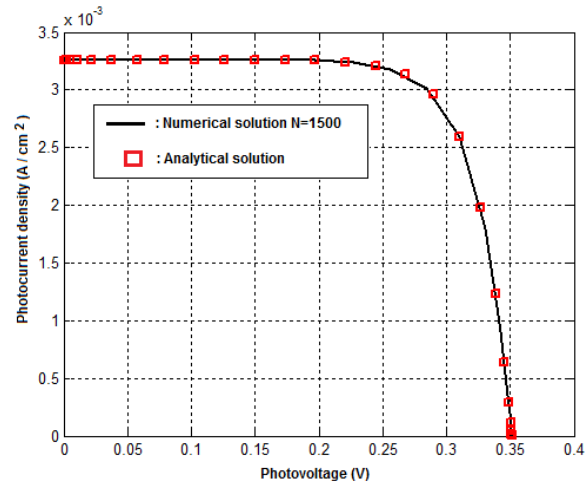


Figure 17. Current-voltage characteristics; $D = 26 \text{ cm}^2/\text{s}$; $L = 0.01 \text{ cm}$; $Sb = 10^3 \text{ cm/s}$, back surface illumination.

4. CONCLUSION

In this study, we have used the finite element method to characterize a silicon bifacial solar cell by solving one-dimensional continuity equation. The determination of the excess minority carrier's density according to the base depth, determination of the photocurrent density and the photovoltage according to the junction recombination velocity, and the current-voltage characteristics of the solar cell enable us to show the concordance between the results obtained in this study and those previously obtained using the usual analytical methods. For the minority carrier's density, the convergence is perfect for $N \geq 200$ when the solar cell is illuminated on the front surface, $N \geq 500$ for the back surface and $N \geq 800$ for double illumination. For the photocurrent density, the agreement is good enough when $N \geq 1000$ for the front surface and $N \geq 1500$ for the back surface. That is explained by the fact that the less the solution is linear, the more the step of the discretization must be small, and therefore, the higher number of finite elements is required.

REFERENCES

1. Ly, I., O. H. Lemrabott, B. Dieng, I. Gaye, S. Gueye, M. S. Diouf, and G. Sissoko, "Techniques de détermination des paramètres de recombinaison et le domaine de leur validité d'une photopile bifaciale au silicium polycristallin sous-éclairage multi spectral constant en régime statique," *Revue des Energies Renouvelables*, Vol. 15, No. 2, 187–206, 2012.
2. Gueye, S., H. Ly. Diallo, M. Ndiaye, M. M. Dione, and G. Sissoko, "Effect of the boundary recombination velocity and the grain size at the phenomenological parameters of the monofacial solar cells under multispectral illumination in steady state," *International Journal of Emerging Technology and Advanced Engineering*, Vol. 3, No. 12, 1–8, 2013.
3. Souleymane Dia, F., O. Diasse, R. S. Sam, H. L. Diallo, B. Dieng, N. Thiam, S. Mbodji, and G. Sissoko, "1D modeling study of series and shunt resistances of silicon solar cell in steady state operating condition and under polychromatic illumination," *International Journal of Advanced Technology & Engineering Research*, Vol. 2, No. 6, 18–23, 2012.
4. Hamidou, A., A. Diao, S. A. Douani, A. Moissi, M. Thiame, F. Barro, and G. Sissoko, "Capacitance determination of a vertical parallel junction solar cell under multispectral illumination in steady state," *International Journal of Innovative Technology and Exploring Engineering*, Vol. 2, No. 3, 1–4, 2013.

5. Nzonzolo, D. Lilonga-Boyenga, and G. Sissoko, "Illumination level effects on macroscopic parameters of a bifacial solar cell," *Energy and Power Engineering*, Vol. 6, 25–36, 2014.
6. Ern, A., *Aide memoire Eléments Finis*, Dunod, Paris, 2005.
7. Sadiku, M. N. O., *Numerical Techniques in Electromagnetics*, 2nd Edition, Library of Congress Cataloging-in-Publication Data CRC Press, Boca Raton, London, New York, Washington, 2001.
8. Diasse, O., R. S. Sam, H. L. Diallo, M. Ndiaye, N. Thiam, S. Mbodji, and G. Sissoko, "Solar cell's classification by the determination of the specific values of the back surface recombination velocities in open circuit and short-circuit operating conditions," *International Journal of Emerging Trends & Technology in Computer Science*, Vol. 1, No. 3, 2012.
9. El Moujtaba, M. A. O., M. Ndiaye, A. Diao, M. Thiame, I. F. Barro, and G. Sissoko, "Theoretical study of the influence of irradiation on a silicon solar cell under multispectral illumination," *Research Journal of Applied Sciences, Engineering and Technology*, Vol. 4, No. 23, 5068–5073, 2012.
10. Diasse, O., R. S. Sam, H. L. Diallo, M. Ndiaye, N. Thiam, S. Mbodji, and G. Sissoko, "Solar cell's classification by the determination of the specific values of the back surface recombination velocities in open circuit and short-circuit operating conditions," *International Journal of Emerging Trends & Technology in Computer Science*, Vol. 1, No. 3, 55–59, 2012.